Co_2N Nanoparticles Embedded N-doped Mesoporous Carbon as Efficient Electrocatalysts for Oxygen Reduction Reaction

Dakai Guo[a], Zhengfang Tian[b], Jiacheng Wang[c]*, Xuebin Ke[d]*, Yufang Zhu[a,b]*

[a] School of Materials Science and Engineering, University of Shanghai for Science and Technology, Shanghai 200093, P. R. China. Email: zjf2412@163.com [b] Hubei Key Laboratory of Processing and Application of Catalytic Materials, College of Chemical Engineering, Huanggang Normal University, Huanggang City, Hubei Province, 438000, P. R. China.

[c] State Key Laboratory of High Performance Ceramics and Superfine Microstructure, Shanghai Institute of Ceramics, Chinese Academy of Sciences, Shanghai 200050, P. R. China. Email: jiacheng.wang@mail.sic.ac.cn [d] School of Engineering and Computer Science, University of Hull, HU6 7RX, United Kingdom. Email: X.Ke@hull.ac.uk

Abstract: Co-N-C electrocatalysts have attracted great attention in electrocatalytic ORR (oxygen reduction reaction) field. In this work, we propose to prepare Co_2N nanoparticles embedded N-doped mesoporous carbon by a facile method including in situ copolymerization and pyrolysis under NH_3 atmosphere. The results show that more N atoms can be doped in carbon framework by NH_3 pyrolysis, it is also found

that pyrolysis temperature and Co content can influence the ORR performance of samples. The sample prepared by adding Co precursor and pyrolysis at 700 °C has high N content (11.86 at. %) and relative large specific surface area (362 m^2 g^{-1}), and it also exhibited superior electrocatalytic ORR performance in terms of E_{onset} (-0.038 V vs. SCE), $E_{1/2}$ (-0.126 V vs. SCE) and large current density (5.22 mA cm^{-2}). Additionally, the sample also shows better stability and resistance to methanol poisoning than Pt/C catalyst. The synergistic effect of Co-N active centers and hierarchical porous structures contribute the excellent electrocatalytic activity, which are considering as alternative catalysts for ORR in full cells.

Keywords: Cobalt nitrides; Mesoporous carbon; Electrocatalysts; Oxygen reduction reaction

1. Introduction

The energy crisis is becoming increasingly serious and continuously threatening the survival environment. Thus, the development of appropriate and sustainable energy is the most crucial task in current scientific research. Fuel cell, an efficient and environmentally friendly energy conversion device, has shown great potential in applications of domestic electricity or automobile power [1-3]. The oxygen reduction

reaction (ORR) occurred in the cathode shows slow and complex reaction kinetics, and it requires the efficient catalysts to lower the overpotential. The platinum (Pt)-based catalysts have the excellent activity towards ORR, but Pt is expensive and its stability decreases during the ORR, so that the commercialization of fuel cell has been seriously restricted [4-7]. The research and development of low-cost and more effective ORR electrocatalysts which can replace platinum-based catalysts is the crucial point for the commercialization of fuel cell. Nowadays, more and more non-precious metal-based materials have been developed for ORR applications, such as transition metal-N-C materials [8-12], metal oxide-based materials [13, 14], metal sulfides-based materials [15-17] and metal-free materials [18-20].

Among these non-precious metal based catalysts, the metal-N-C catalysts show great potential for ORR since Jasinski et al. studied the ORR catalysis of the cobalt phthalocyanine (CoPc) under alkaline conditions [21]. Gupta et al. later demonstrated that the metal-based N-doped carbon materials obtained by the high-temperature pyrolysis of metal macrocycles could improve ORR activity [22-24].

After these works, more and more M-N-C (M=Fe, Co, etc.) materials are investigated to substitute the precious metal based catalysts towards ORR. These transition metal-N-C catalysts show excellent activity, while the catalytic mechanism for the ORR has not been understood clearly. Some studies demonstrated that the existence of the N atoms in those M-N-C type catalysts could enhance the ORR performance because the N groups could serve as the bridge for connecting the metal active sites and N atoms [25-27]. For example, Fe-N_x moieties have been proved as the main active reaction sites in Fe-based nitrogen-doped carbon materials [28]. The Co-N-C catalysts also

show excellent ORR activity due to the Co-N moieties (Co-N_2, Co-N_4). Amiinu et al. reported Co–N_x/C nanorod array with superior electrocatalytic activity and stability toward ORR compared to commercial Pt/C, and it has been proved that the improved activity of Co-Nx/C nanorod is attributed to the synergistic effects of the Co-N moieties [29]. Wang et al. prepared nitrogen-doped carbon nanotubes with the encapsulation of Co nanoparticles (Co-N-CNTs) for ORR and OER application. Specifically, the excellent ORR performance is also derived from those highly active Co-N-C moieties [30]. Besides, the Co-N-C moieties are also effective for other reactions, such as the selective oxidation of alkylaromatics [31]. Additionally, Co-based materials like CoO- [32], Co_3O_4- [33] and Co_xS_{1-x}-based [34] carbon supported catalysts also exhibit outstanding ORR activity. Recently, a study indicated that the enhanced ORR performance of the Co-N-C catalyst might be caused by the formation of some cobalt-based species including cobalt oxides, cobalt carbides and metallic cobalt. It could be speculated that there is a synergistic reaction between the Co-N moieties and cobalt-based species [35]. Some Co-based catalysts even show better activity than commercial Pt/C catalysts. Guo et al. synthesized the cost-effective Co-N,B-CSs catalyst by soft template self-assembly pyrolysis method, and the DFT calculations further demonstrated that the coupling of Co-N_x active sites with B atoms could accelerate ORR kinetics [36]. Wu et al. prepared porous CoN_x/C materials via pyrolysis at high temperatures (Ar/N_2) by using $Co(NO_3)_2$ precursor and MWCNT (N source) [37]. The resulting catalyst showed enhanced ORR activity and stability due to the high-speed electron transmission and high electroconductivity of graphitic carbon. Xia et al. synthesized the Co/N-doped CNTs (NCNTs) composite via the direct pyrolysis (Ar/H_2,

90%/10%) of a Co-based MOF (ZIF-67), which also shows excellent ORR activity [38]. Zhou et al. synthesized novel MOF-derived carbon nanotubes (Co/N-CNTs) with $mSiO_2$-coated ZIF-67 nanocrystal, and the catalyst showed excellent ORR activity and stability [39]. Consequently, it is important how to design and synthesize efficient Co-N-C catalyst, much work still need to be performed to understand the reaction mechanisms for ORR in those catalysts.

In this work, we report a simple method to prepare cobalt nitride (Co_2N) nanoparticles embedded N-doped mesoporous carbon framework for ORR. In our strategy, the Co salt ($Co(NO_3)_2{\cdot}6H_2O$) is served as Co source and the Co^{2+} could be adsorbed by the copolymers of aniline and pyrrole (polymer spheres) due to the charge interaction. On the other hand, the polymer spheres could be also served as N source and C source during the synthesis. It has been proved that pyrolysis under NH_3 atmosphere could increase the total N content in carbon framework, and make more N atoms combining with Co dopants to form Co-N moieties (Co_2N nanoparticles), and thereby enhance the ORR activity [40]. The existence of Co_2N nanoparticles in composites create more ORR active sites and speed up the adsorption/reaction of oxygen. Additionally, mesoporous carbon structure is considered to benefit charge transmission and mass diffusion during the whole period. For these unique properties, the as-prepared Co-N-C (Co_2N-2-700@NC) catalysts show the superior ORR activity comparable to commercial Pt/C, besides, the durability, tolerance to methanol crossover, half-wave potential under the alkaline conditions are even better than those of Pt/C catalysts.

2. Experimental

2.1 Materials and chemicals

Anhydrous ethanol (EtOH), ammonium persulfate (APS) [$(NH_4)_2S_2O_8$, ≥ 98%], Triton X-100 [C_6H_4-$(OCH_2CH_2)_nOH$, n=9-10], cobalt (II) nitrate hexahydrate [$Co(NO_3)_2{\cdot}6H_2O$, (≥ 99.9%)], pyrrole (≥ 99%) and aniline (≥ 99%) were purchased from Sinopharm Co. Ltd., the commercial Pt/C catalyst (20 wt%) was purchased from Johnson Matthey (UK), Nafion solution (5 wt%) were purchased from Sigma (China). Milli-Q ultrapure water was used during the whole experimental process.

2.2 Synthesis of Co_2N-x-T@NC electrocatalysts

The synthesis procedure of electrocatalysts is shown as follows. 0.40 ml aniline, 0.30 ml pyrrole, 0.06 g emulsifier (Triton X-100) and a certain amount of $Co(NO_3)_2{\cdot}6H_2O$ were dissolved in 60 ml deionized water, and this mixture was maintained at 5 °C for 1 hour before copolymerization. Then the precooled APS aqueous solution (0.05 g/ml) was added into the above solution for cationic polymerization for 48 h (maintain at 5 °C) to obtain precursors. Subsequently, the precursors were washed with DI water until the filtration became colorless, then drying at 50 °C for 12 h. The obtained precursors were pyrolyzed under NH_3 atmosphere at 600-800 °C for 2h (5 °C min^{-1}) to synthesize Co_2N-x-T@NC. Here, x represents the amount of $Co(NO_3)_2{\cdot}6H_2O$ (x=1, 2 or 3 mmol) and T represents the pyrolysis temperature (T=600, 700 or 800 ^oC). For comparison, precursors synthesized

without $Co(NO_3)_2 \cdot 6H_2O$ were pyrolyzed under N_2 atmosphere at 700 °C to obtain PCM-700 electrocatalysts.

2.3 Characterization

XRD patterns of electrocatalysts were obtained by a D8 ADVANCE powder diffractometer. SEM images of electrocatalysts were observed with a scanning electron microscope (FEI Quanta 450), TEM images were obtained by a transmission electron microscope (300 kV, Tecnai G2 F30). Raman Microscopy was used to obtain Raman spectra. XPS spectra were obtained by an ESCALAB 250 spectrometer. Nitrogen sorption isotherms were measured on Micromeritics Tristar II 3020 at -196 °C for calculating specific surface areas based on Brunauer–Emmett–Teller (BET) theory, while the pore size distribution was obtained based on Barrett–Joyner–Halenda (BJH) model.

2.4 Electrode preparation and electrochemical measurements

The electrocatalytic performances were performed with a three-electrode system in 0.1 M KOH electrolyte (Pine Co.). A saturated calomel electrode (SCE) was served as the reference electrode and a Pt sheet (1×1 cm) was served as the counter electrode. The polished modified glassy carbon (GC) electrode (RDE and RRDE) were used as the working electrode (5 mm). For the preparation of ink, 5 mg of sample, 500 μL of deionized water, 500 μL of anhydrous ethanol and 20 μL of Nafion were mixed by ultrasonic method for 1 h to form a uniform dispersion. After that, 20 μL of catalyst ink was dropped onto the surface of GC electrode by a micro injector, then dried at 60 °C for several minutes. A Pt/C working electrode was prepared via the same method.

Specially, the electrolyte should be purged by oxygen or nitrogen for 30 min before tests.

Before collecting results, the working electrode was activated in O_2-saturated electrolyte by CV measurement (0.1 to -1 V vs. SCE, speed: 100 mV s^{-1}). Linear sweep voltammetry (LSV) measurements were performed (0.1 to -1 V vs. SCE, speed: 10 mV s^{-1}, 400 to 1600 rpm). The current densities obtained from LSV tests were normalized to the geometric surface area. The number of transferred electrons (n) could be obtained using the Koutecky-Levich (K–L) equation (1) and (2):

$$\text{– – ———} \quad _2 \qquad (\ )$$

$$0.2nFCo_2Do_2^{2/3}\upsilon^{-1/} \qquad (2)$$

where J represents the measured current density, J_k represents the kinetic current density, represents the rotation speed (in rpm), n represents the number of transferred electrons, F (Faraday constant) is equal to 96485 C mol^{-1}, Co_2 is the bulk concentration of oxygen (1.2×10^{-6} mol cm^{-3}), Do_2 is the diffusion coefficient of dissolved oxygen (1.9×10^{-5} cm^2 s^{-1}), is equal to 0.01 cm^2 s^{-1}.

For the RRDE test, a glass carbon electrode (the disk was encircled by a Pt ring) was employed. The RRDE tests were conducted by LSV measurement from 0.1 to -1 V vs. SCE in O_2-saturated 0.1 M KOH (scan rate: 10 mV s^{-1}) at 1600 rpm for collecting the ring current and disk current (the ring potential: 0.2 V vs. SCE). The H_2O_2 yields (%) and the electron transfer number (n) can be calculated by using the equation (3) and (4):

/

$$_{2}\ 200\ \ \frac{_{r}N}{_{d\ r}N\ ^{d}n} \qquad (\ )$$

$$_{d\ r}N \qquad (\ )$$

in which I_d represents the disk current, Ir represents the ring current, N = 0.37.

The durability and methanol tolerance performance of Co_2N-2-700@NC and 20 wt% Pt/C were evaluated by chronoamperometric (CA) method at -0.6 V vs. SCE.

3. Results and discussion

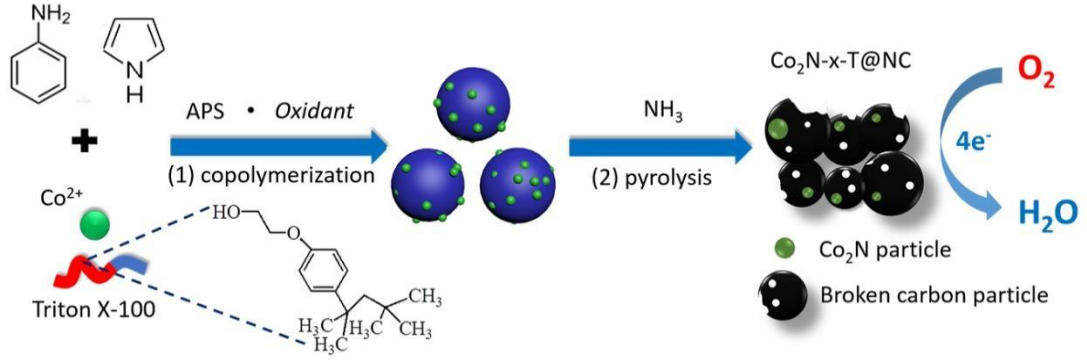

Figure 1. Scheme for the synthesis of Co_2N-x-T@NC: (1) Copolymerization of Co^{2+}-Aniline-Pyrrole system; (2) Pyrolysis of the precursors under NH_3 atmosphere at 600-800 °C.

Figure 1 shows the synthesis process of Co_2N-x-T@NC electrocatalysts. In step (1), the aniline and pyrrole co-monomers were located in the different position of the Triton X-100 micelles: the aniline molecules were located in the outsides (micelle-water interface) due to its amphiphilic characteristic; the pyrrole molecules were located in the interiors of micelles due to its hydrophobic characteristic. The polymerization first occurred at outsides because the oxidant (APS) is hydrophilic. Afterwards, the diffusion of the pyrrole monomers from interiors to outsides continue to promote the reaction process, resulting in the formation of polymer spheres [41].

Meanwhile, Co^{2+} ions were adsorbed by those copolymers under the charge interaction [9]. The APS serves as the initiator for the copolymerization of aniline-pyrrole-Co^{2+} system, while the residual APS would be removed during the following centrifugation and washing process. In step (2), the obtained precursors, polymer spheres, were pyrolyzed under NH_3 atmosphere at 600-800 °C. It has been proved that pyrolysis of the carbon-based materials under NH_3 atmosphere could introduce more nitrogen atoms into carbon substrate and increase the total nitrogen content. After the pyrolysis process, polymer spheres could be converted to the broken mesoporous carbon particles due to the high-temperature pyrolysis, meanwhile, a certain amount of metal nitride (Co_2N) nanoparticles embedded in mesoporous carbon were formed during the pyrolysis under NH_3 atmosphere.

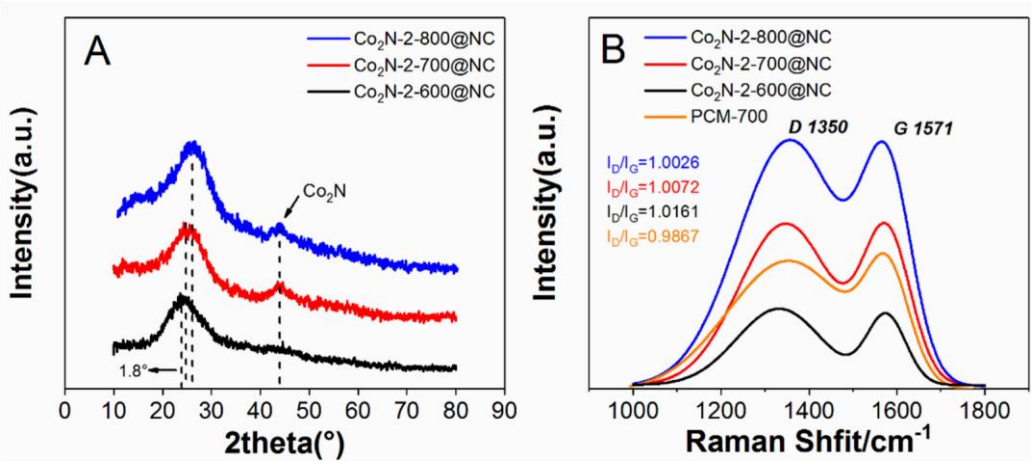

Figure 2. (A) XRD patterns of Co_2N-2-T@NC (T=600, 700, 800); (B) Raman spectra of Co_2N-2-T (T=600, 700, 800) and PCM-700

The crystal structures of the Co_2N-2-600@NC, Co_2N-2-700@NC and Co_2N-2-800@NC were studied by XRD analysis in Figure 2A. The peak at 24.1 ° in the XRD pattern of Co_2N-2-600@NC indicates its amorphous structure. With the temperature increased to 800 °C, it can be found that this peak of Co_2N-2-800@NC

shifts positively to 26.2 °, which is in agreement with the (002) crystal face of graphitic carbon structure. The peaks at about 44.5 ° could be assigned to the (021) crystal face of Co_2N (JCPDS: No. 06-0647) [42]. Besides, it is clear that the intensities of the peaks increased with the pyrolysis temperature increased. The peak intensity of Co_2N-2-600 is the weakest, proving that the crystallization of Co_2N-2-600 is lower than other two samples, and it is known that high crystallization could enhance the catalytic ability of nanocrystals. For comparison, the XRD patterns of samples synthesized with different amount (1 mmol, 2 mmol and 3 mmol) of $Co(NO_3)_2 \cdot 6H_2O$ and pyrolyzed at 700 °C were shown in Figure S1. It can be found that the peak intensity of Co_2N phase increases with the increase of Co^{2+} content. These XRD results indicate that all samples are consisted of Co_2N nanoparticles and amorphous/graphitic carbon structures.

Raman spectra of Co_2N-2-600@NC, Co_2N-2-700@NC and Co_2N-2-800@NC are shown in Figure 2B to investigate the differences of microstructure among these samples. The peaks at 1350 cm^{-1} (D band) are related to the defect in graphitic carbon framework while the other peaks at 1571 cm^{-1} (G band) represents the E_{2g} vibration of carbon atoms. From the results of D bands in those Raman curves, it could be speculated that there exists a certain amount of defects possibly caused by the introduction of nitrogen atoms into carbon frameworks during the pyrolysis under NH_3 atmosphere. The graphitic degree of samples could be evaluated by calculating the intensity ratios (I_D/I_G). The ratio for Co_2N-2-600@NC, Co_2N-2-700@NC and Co_2N-2-800@NC are 1.0161, 1.0072 and 1.0026, respectively. Combining the previous XRD results, it is easily found that the graphitic degree of these samples increases with the

pyrolysis temperature increases. Carbon structures with high graphitic degree are beneficial for enhancing the electrocatalytic activity owing to the high electrical conductivity.

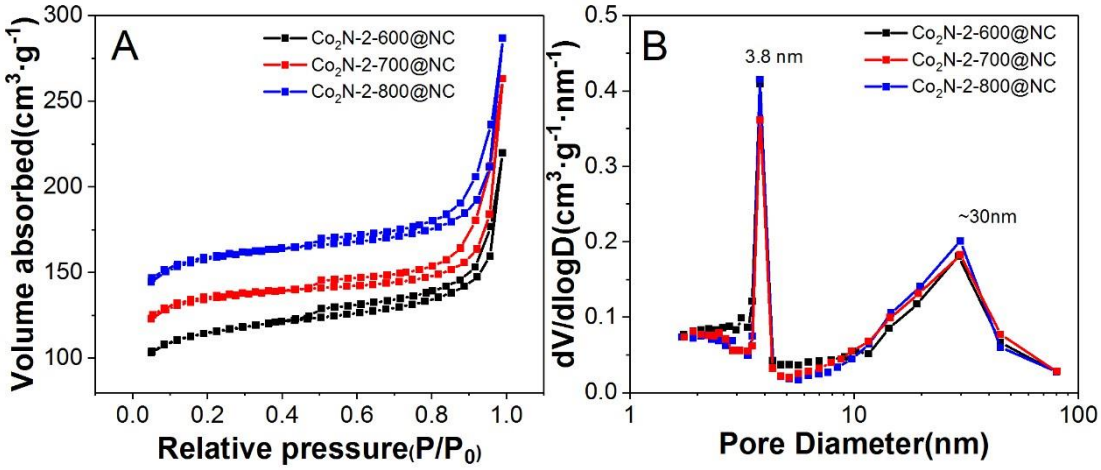

Figure 3. (A) The N_2 sorption isotherms and (B) the corresponding BJH pore-size distribution curves for Co_2N-2-T@NC (T=600, 700, 800).

N_2 adsorption-desorption measurements were used to analyze the BET surface area and pore texture of these samples. The distinct hysteresis loops (type IV) could be found in these isotherms of all three samples (Figure 3A), indicating the existence of mesopores in Co_2N-2-T@NC (T=600, 700, 800). And the specific surface areas of the Co_2N-2-600@NC, Co_2N-2-700@NC and Co_2N-2-800@NC are 247, 362 and 424 m^2/g, respectively. Figure 3B exhibits the pore size distributions of these three samples. The narrow peaks at 3.8 nm and peaks at ca. 30 nm are observed in all three samples, which may be attributed to the gas generation and the breaking of some polymer spheres during the pyrolysis period. Small mesopores (3.8 nm) could lower the transmission resistance of the reactants towards ORR, while large mesopores (~30 nm) could store the electrolyte and accelerate the reaction rate. Thus, it can be speculated that relative high BET surface area and hierarchical structure in these samples could

produce more active sites and provide more reaction places, and thereby promote the transmission rate of electrolyte, reactants, and products in ORR [43].

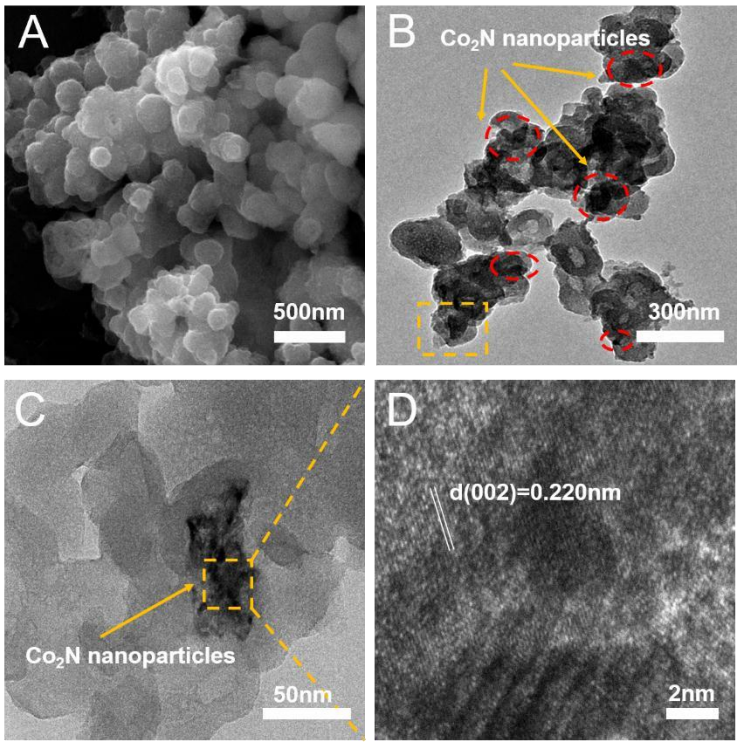

Figure 4. (A) SEM image, (B, C) TEM images and (D) HRTEM image of Co_2N-2-700@NC.

Figure 4A shows the SEM image of Co_2N-2-700@NC. Most of Co_2N-2-700@NC particles are spherical, but a small amount of broken fractal particles is also observed due to the high temperature pyrolysis. These broken/spherical carbon particles could offer the mesopores. Figure 4B confirmed that cobalt nitride nanoparticles (circled by red line) were embedded in mesoporous carbon framework. As shown in Figure 4C-D, the lattices fringes with distance of 0.22 nm agree well with the (002) plane of Co_2N [42]. These SEM and TEM results are in consistent with previous XRD patterns. SEM and TEM images of PCM-700 electrocatalysts without the Co addition (Figure S2) showed that the PCM-700 nanoparticles are almost spherical and the particle size ranges from 70 to 100 nm. The addition of Co precursor influenced the

micromorphology of those final electrocatalysts slightly. On the other hand, little differences in the morphology and particle size can be found for Co_2N-2-600@NC, and Co_2N-2-800@NC electrocatalysts compared to Co_2N-2-700@NC electrocatalysts (Figure S3).

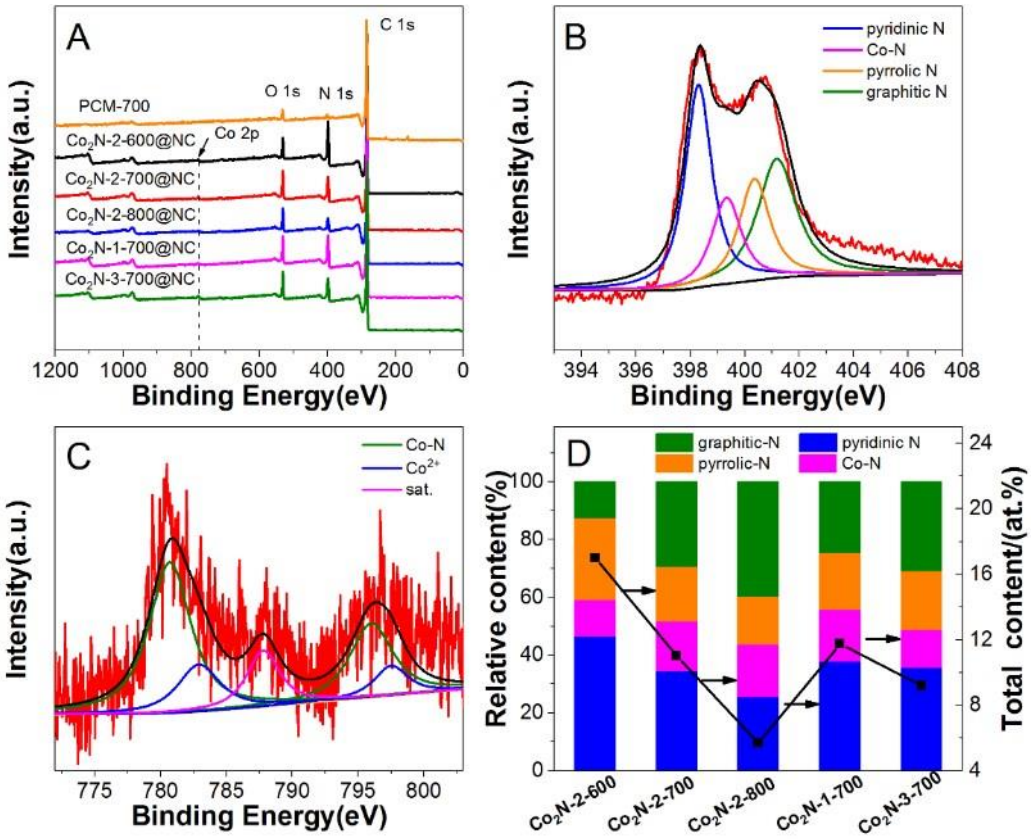

Figure 5. (A) XPS spectra of Co_2N-x-T@NC and PCM-700; (B, C) High-resolution N 1s and Co 2p XPS spectra of Co_2N-2-700@NC, respectively; (D) Total N content and N bonding configurations of Co_2N-x-T@NC.

XPS measurements were conducted to investigate the element composition of the surface and obtain some information about bonding configurations of Co_2N-x-T@NC. The samples Co_2N-x-T@NC show C 1s peaks (~284 eV), O 1s peaks (~530 eV), N 1s peaks (~400 eV) and Co 2p peaks (~780 eV) in the XPS spectra (Figure 5A), and sample PCM-700 shows weak N 1s peak due to its low N content. The high

resolution N 1s XPS spectrum of Co_2N-2-700@NC are divided into four peaks, and the peaks appeared (Figure 5B) at 398.3, 401.2, 399.3 and 400.3 eV were ascribed to pyridinic N, graphitic N, Co-N bond and pyrrolic N, respectively [44]. For Co 2p spectrum in Figure 5C, two distinct peaks (green line) at about 780.8 and 796.0 eV are corresponding with Co-N bond [42]. These results (N 1s and Co 2p spectrum) indicate the existence of the Co-N structure in the synthesized Co_2N-2-700@NC electrocatalysts. The N 1s spectra of other as-prepared samples (Co_2N-1-700@NC, Co_2N-3-700@NC, Co_2N-2-600@NC and Co_2N-2-800@NC) are also compared and displayed in Figure S4A-D. Obviously, the N bonding configurations and total N content of those samples show some differences. It has been reported that graphitic N can enlarge the current density and pyridinic N can make the E_{onset} more positive for ORR [45]. In Co-N-C system electrocatalysts, the existence of Co-N bond also plays a critical role in ORR electrocatalysis. The sample Co_2N-2-600@NC has the highest total nitrogen content but the low content of Co-N bond and graphitic N; the sample Co_2N-2-800@NC has relative high content of graphitic N, but the total nitrogen content is the lowest among these samples, which would lower the ORR activity. The N bonding configurations and total N content of other two samples (Co_2N-1-700@NC and Co_2N-3-700@NC) are close to the sample Co_2N-2-700@NC. Moreover, the elemental atomic ratios of those samples detected by XPS measurement are shown in Table S1. It is also obvious that those samples contain a certain amount of N (6.02-17.89%) and Co (0.456-1.172%), which proves the N-doping and Co_2N in Co_2N-x-T@NC electrocatalysts.

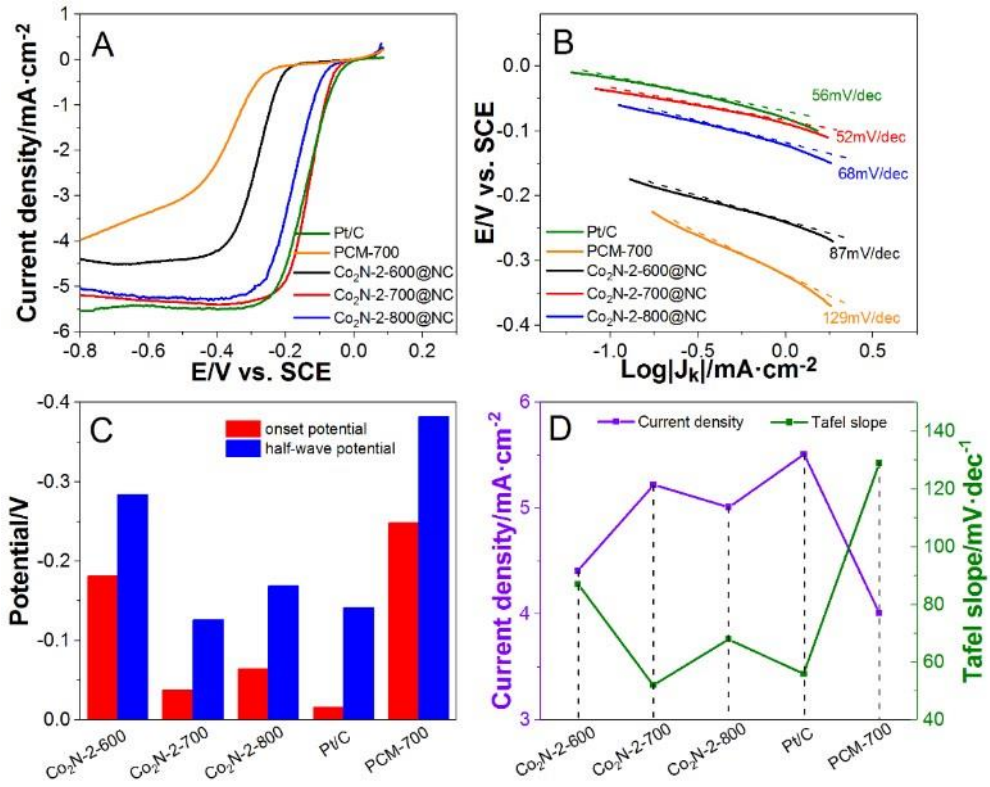

Figure 6. (A) LSV curves of Co_2N-2-T@NC (T= 600, 700, 800), Pt/C and PCM-700 in O_2-saturated 0.1 M KOH solution at 1600 rpm; (B) Tafel plots derived from Figure 6A; (C) Comparisons of E_{onset} and $E_{1/2}$ for PCM-700, Co_2N-2-T@NC (T= 600, 700, 800) and Pt/C; (D) Comparisons of current densities and Tafel slopes for Co_2N-2-T@NC (T= 600, 700, 800), Pt/C and PCM-700, respectively.

For the electrocatalysis tests, circle voltammetry (CV) measurements were conducted via the RDE technique in O_2-saturated 0.1 M KOH electrolyte to study the ORR activity. CV curves of Co_2N-2-700@NC are shown in Figure S5, and an obvious cathodic peak appeared under O_2-saturated condition, however, no related peak could be found under N_2-saturated condition, such a result proves the effective ORR activity for Co_2N-2-700@NC. Figure S6A shows the CV curves of Co_2N-2-600@NC and Co_2N-2-800@NC. It is obviously found that the peak of Co_2N-2-700@NC is more positive than Co_2N-2-600@NC and Co_2N-2-800@NC synthesized at other temperatures, because the

increase of temperature could improve the BET surface area of samples effectively to generate more active sites and promote the reaction rate, on the other hand, the increase of temperature could improve the crystallinity of Co2N nanoparticles, thus enhancing the ORR performance. However, it is known that the content of nitrogen could decrease with the increase of temperature and the decrease of nitrogen content could influence the ORR activity. In our work, it is noticed that Co_2N-2-800@NC shows lower ORR activity than Co_2N-2-700@NC. Combined with the XRD and XPS results, it can be seen that the crystallinity of these two samples are similar, but the total N content and relative Co-N content of Co_2N-2-800@NC is lower than Co_2N-2-700@NC, so that the sample Co_2N-2-700@NC should show the better ORR performance.

Additionally, it can be found in the Figure 5D that the bonding configurations of nitrogen for those samples are different, the graphic-N content and Co-N typed N content of Co_2N-2-600@NC are less than Co_2N-2-700@NC. It has been proved that the relative high content of graphic-N/pyridinic-N/Co-N could improve the ORR performance. Besides, the crystallinity of Co_2N-2-700@NC is higher than Co_2N-2-600@NC, the higher crystallinity of Co_2N nanoparticle could also enhance the ORR activity. [46].

LSV curves of PCM-700, Co_2N-2-T@NC (T= 600, 700, 800) and Pt/C and are exhibited and compared in Figure 6A. The comparison of their onset potential (E_{onset}) and half-wave potential ($E_{1/2}$) are shown in Figure 6C. The Co_2N-2-700@NC exhibits the best performance (Figure 6C) with an E_{onset} of -0.038 V vs. SCE and a $E_{1/2}$ of -0.126 V vs. SCE, which are similar to Pt/C (-0.016 and -0.141V vs. SCE). The E_{onset} and $E_{1/2}$ of

Co_2N-2-700@NC are much more positive than those of Co_2N-2-600@NC (-0.181 and -0.284 V vs. SCE), Co_2N-2-800@NC (-0.064 and -0.169 V vs. SCE) and PCM-700 (-0.248 and -0.382 V vs. SCE). Besides, Tafel plots derived from Figure 6A are also compared in Figure 6B. Among these samples, the Tafel slope of Co_2N-2-700@NC is the smallest (52 mV), superior than Pt/C (56 mV), which suggests the excellent reaction dynamics towards ORR. Figure 6D shows that the limiting current density of Co_2N-2-700@NC (5.22 $mA \cdot cm^{-2}$) is smaller than that of Pt/C (5.51 $mA \cdot cm^{-2}$) slightly, but much larger than that of PCM-700 (4.01 $mA \cdot cm^{-2}$), Co_2N-2-600@NC (4.41 $mA \cdot cm^{-2}$) and Co_2N-2-800@NC (5.01 $mA \cdot cm^{-2}$), confirming the synergistic effect of cobalt nitrides (Co_2N) and mesoporous carbon. Figure S7A shows the effect of the Co content in electrocatalysts on the ORR performance of Co_2N-x-700@NC (x= 1, 2, 3). The LSV curves demonstrate that suitable Co addition (2 mmol) result in the best ORR performance. Too many Co addition (3 mmol) could lower the relative content of Co-N (Co_2N) bond and graphitic N and increase the relative content of metal Co (the metal Co shows weaker catalytic ability than Co-N active sites toward ORR) [47]. Furthermore, to study the influence of NH_3/N_2 pyrolysis and Co/N doping in these Co-N-C electrocatalysts, the LSV curves of sample PCM-700(NH_3) pyrolyzed in NH_3 atmosphere and Co_2N-2-700(N_2)@NC pyrolyzed in N_2 atmosphere were also investigated and compared in Figure S7B. Co_2N-2-700@NC pyrolyzed in NH_3 atmosphere shows the best ORR performance (the most positive E_{onset} and $E_{1/2}$) among those three samples, so it is clear that the Co doping and NH_3 pyrolysis could enhance the ORR activity in these Co-N-C samples. It can be concluded that there are three key factors determining the electrocatalytic

performance for Co_2N-2-700@NC: (i) Co_2N as the main active sites: it has been proved that Co-N species are main ORR active sites in Co-N-C system electrocatalysts. (ii) Reasonable content of Co source and pyrolysis under NH_3 atmosphere: pyrolysis in NH_3 atmosphere could introduce a certain amount of nitrogen atoms into the final carbon framework, the high relative nitrogen content is also benefit for the formation of Co-N moieties [48]. (iii) Graphitic-N and pyridinic-N configuration: the charge and spin properties of carbon atoms could be tuned and adjusted by nitrogen-doping, especially for graphitic-N and pyridinic-N, which can enhance the surface-adsorption of reaction intermediates on carbon frameworks and lower the binding energy between electrocatalysts and reactants, thus improving the ORR performance of N-doping carbons. As shown in Table S2, Co_2N-2-700@NC is also superior to many Co-N-C electrocatalysts towards the ORR reported by other literatures.

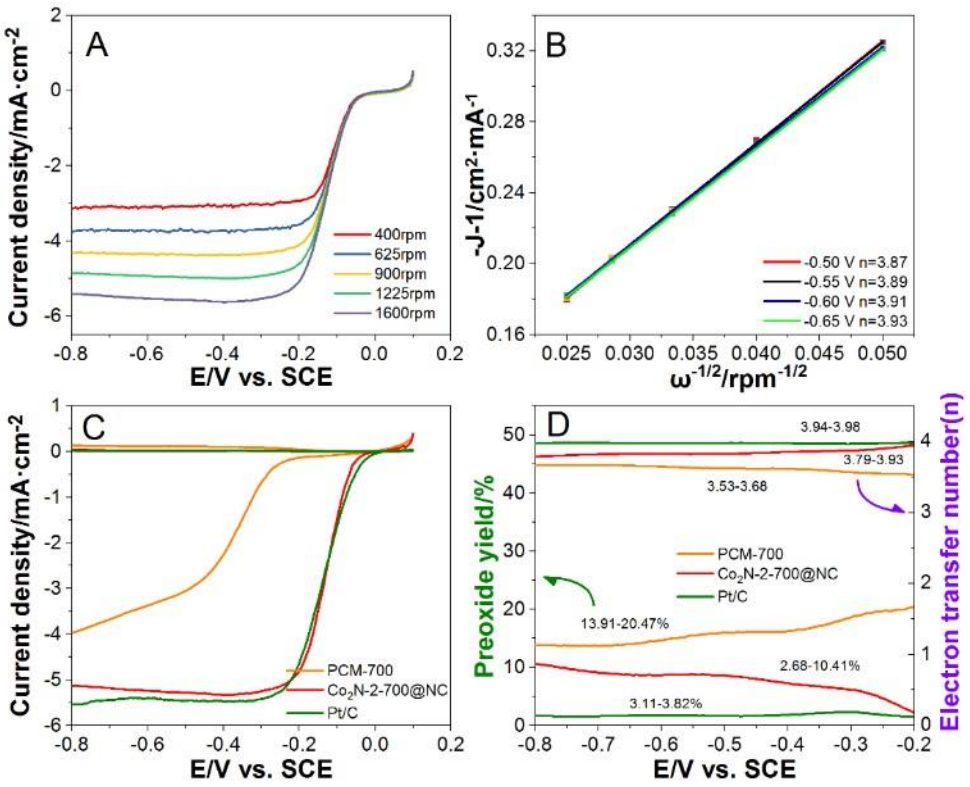

Figure 7. (A) LSV curves of Co_2N-2-700@NC in O_2-saturated 0.1 M KOH electrolyte

(400-1600 rpm); (B) K-L plots at different potentials; (C) RRDE voltammograms for PCM-700, Co_2N-2-700@NC and 20wt% Pt/C (1600 rpm, ring potential: 0.2 V vs. SCE); (D) The calculated H_2O_2 yield (%) and electron transferred number (n) from RRDE results (-0.8 to -0.2 V vs. SCE).

To investigate the reaction dynamics of ORR, LSV curves of Co_2N-2-700@NC in O_2-saturated 0.1 M KOH electrolyte at the rotation speed from 400 to 1600 rpm were tested by the RDE (Figure 7A). Figure 7B shows the K-L plots (-0.5 to -0.65 V vs. SCE). The numbers of transferred electrons (3.87-3.93) obtained by K-L plots for Co_2N-2-700@NC were close to that of Pt/C, indicating the direct $4e^-$ ORR reaction pathway. The RRDE measurements were used to detect the transfer electron number and H_2O_2 yields during the reaction period. As shown in Figure 7C, RRDE voltammograms for PCM-700, Co_2N-2-700@NC and Pt/C were given to calculate the number (n) of transferred electrons and H_2O_2 yields (%) for those samples (Figure 7D), Co_2N-2-700@NC shows n (3.79-3.93) and peroxide yields (2.68-10.41%) over the potential (-0.2 to -0.8 V vs. SCE), consistent with the n values obtained from the Koutecky-Levich plots. The numbers of transferred electrons and H_2O_2 yields of Co_2N-2-700@NC are very close to Pt/C (3.94-3.98; H_2O_2 yields: 3.11-3.82%), superior to those for PCM-700 (3.53-3.68; H_2O_2 yields: 13.91-20.47%), demonstrating the combination of cobalt nitrides and nitrogen-doping via NH_3 pyrolysis obviously improves the ORR activity.

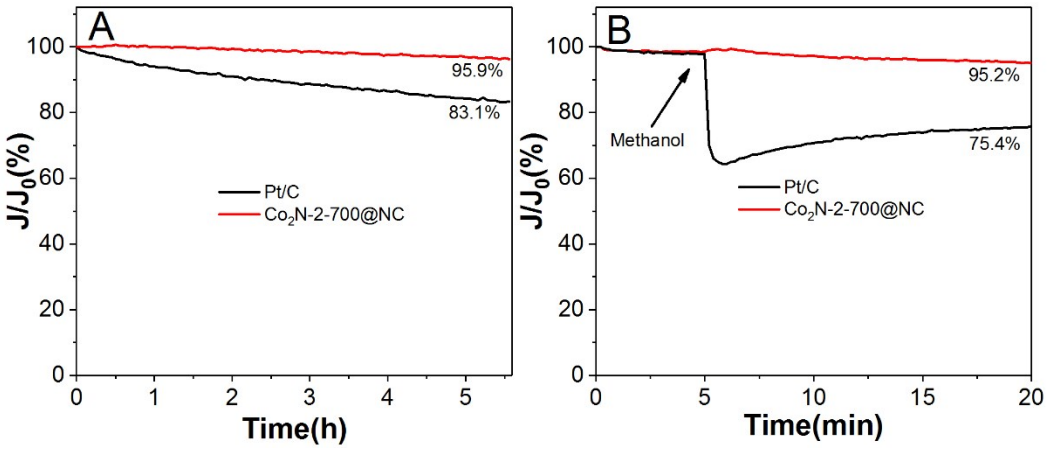

Figure 8. (A) Current–time chronoamperometric responses (CA) for Co_2N-2-700@NC and 20 wt% Pt/C at -0.6 V vs. SCE (1600 rpm); (B) CA measurements of Co_2N-2-700@NC and Pt/C with 3 M methanol added at 300s.

To study the ORR durability and methanol toleration of Co_2N-2-700@NC and Pt/C, chronoamperometric responses measurements were conducted in O_2-saturated electrolyte (1600 rpm) with the potential maintained at -0.6 V vs. SCE. As shown in Figure 8A, Co_2N-2-700@NC exhibits much better stability (95.9% remaining) than Pt/C (83.1% remaining) after test. On the other hand, compared to the Co_2N-2-700@NC before ORR process (Figure 4), little difference can be observed from the SEM and TEM images of the Co_2N-2-700@NC after ORR process (Figure S8), also suggesting the stability of the Co_2N-2-700@NC toward ORR. As shown in Figure 8B, after the injection of methanol (6 mL), the current density of Co_2N-2-700@NC shows slight variations but finally remain stable (95.2% remaining), conversely, the current density of Pt/C decrease significantly (75.4% remaining) due to the CH_3OH oxidation reaction [49]. Based on those above results, Co_2N-2-700@NC shows more excellent durability and methanol toleration than Pt/C catalysts.

4. Conclusions

In this study, we successfully prepared cobalt nitride nanoparticles embedded N-doped mesoporous carbon by introducing the Co sources into polymer spheres and pyrolysis under NH_3 atmosphere at high temperature. The optimized Co_2N-2-700@NC electrocatalyst shows a direct $4e^-$ reaction process and the E_{onset} and $E_{1/2}$ are also close to or even better than Pt/C catalyst. Additionally, Co_2N-2-700@NC electrocatalyst exhibits preferable stability and better methanol toleration. The combination and synergistic reaction of cobalt nitrides nanoparticles and N-doped mesoporous carbon contribute those outstanding electrocatalytic performances. The formation of cobalt nitrides and N-doping are benefit for providing more active sites in Co-N-C electrocatalysts, while relatively high BET surface area and mesoporous structure could expedite the process of mass diffusion and the transmission of reactants/products/electrolyte. Therefore, the Co_2N nanoparticles embedded N-doped mesoporous carbon are promising as alternative catalysts in fuel cell fields.

Acknowledgements

The authors are grateful to the financial support from the National Natural Science Foundation of China (51572172), the National Key Research and Development Program of China (2016YFB0700204), and One Hundred Talent Plan of Chinese Academy of Sciences.

References

[1] M.K. Debe, Electrocatalyst approaches and challenges for automotive fuel cells, Nature 486 (2012) 43.

[2] R. Bashyam, P. Zelenay, A class of non-precious metal composite catalysts for fuel cells, Nature 443 (2006) 63.

[ ] L. ang Soo, T. . Sun, C. Ruiguo, C. Nam Soon, L. Meilin, L. . Tae, C. aephil, Metal–Air Batteries with High Energy Density: Li–Air versus Zn–Air, Adv. Energy Mater. 1 (2011) 34-50.

[ ] W. Xia, A. Mahmood, Z. Liang, R. Zou, S. Guo, Earth Abundant Nanomaterials for Oxygen Reduction, Angew. Chem. Int. Ed. 55 (2015) 2650-2676.

[5] A. Morozan, B. Jousselme, S. Palacin, Low-platinum and platinum-free catalysts for the oxygen reduction reaction at fuel cell cathodes, Energy Environ. Sci. 4 (2011) 1238-1254.

[6] Y. Nie, L. Li, Z. Wei, Recent advancements in Pt and Pt-free catalysts for oxygen reduction reaction, Chem. Soc. Rev. 44 (2015) 2168-2201.

[7] F.T. Wagner, B. Lakshmanan, M.F. Mathias, Electrochemistry and the Future of the Automobile, J. Phys. Chem. Lett. 1 (2010) 2204-2219.

[8] T. Zhou, R. Ma, T. Zhang, Z. Li, M. Yang, Q. Liu, Y. Zhu, J. Wang, Increased activity of nitrogen-doped graphene-like carbon sheets modified by iron doping for oxygen reduction, J. Colloid Interface Sci. 536 (2019) 42-52.

[9] G. Wu, K.L. More, C.M. Johnston, P. Zelenay, High-Performance Electrocatalysts for Oxygen Reduction Derived from Polyaniline, Iron, and Cobalt, Science 332 (2011) 443-447.

[10] T. Zhou, Y. Zhou, R. Ma, Q. Liu, Y. Zhu, J. Wang, Achieving excellent activity and stability for oxygen reduction electrocatalysis by hollow mesoporous iron-nitrogen-doped graphitic carbon spheres, J. Mater. Chem. A 5 (2017) 12243-12251.

[11] D. Guo, S. Han, J. Wang, Y. Zhu, MIL-100-Fe derived N-doped Fe/Fe_3C@C electrocatalysts for efficient oxygen reduction reaction, Appl. Surf. Sci. 434 (2018) 1266-1273.

[12] S. Han, X. Hu, J. Wang, X. Fang, Y. Zhu, Novel Route to Fe-Based Cathode as an Efficient Bifunctional Catalysts for Rechargeable Zn–Air Battery, Adv. Energy Mater. 8 (2018) 1800955.

[13] P. Li, R. Ma, Y. Zhou, Y. Chen, Z. Zhou, G. Liu, Q. Liu, G. Peng, Z. Liang, J. Wang, In situ growth of spinel $CoFe_2O_4$ nanoparticles on rod-like ordered mesoporous carbon for bifunctional electrocatalysis of both oxygen reduction and oxygen evolution, J.

Mater. Chem. A 3 (2015) 15598-15606.

[14] P. Li, R. Ma, Y. Zhou, Y. Chen, Q. Liu, G. Peng, J. Wang, The direct growth of highly

dispersed CoO nanoparticles on mesoporous carbon as a high-performance electrocatalyst for the oxygen reduction reaction, RSC Adv. 6 (2016) 70763-70769.

[15] R. Li, Y. Dai, B. Chen, J. Zou, B. Jiang, H. Fu, Nitrogen-doped Co/Co_9S_8/partly-graphitized carbon as durable catalysts for oxygen reduction in microbial fuel cells, J. Power Sources 307 (2016) 1-10.

[16] M. Shen, C. Ruan, Y. Chen, C. Jiang, K. Ai, L. Lu, Covalent Entrapment of

Cobalt–Iron Sulfides in N-Doped Mesoporous Carbon: Extraordinary Bifunctional

Electrocatalysts for Oxygen Reduction and Evolution Reactions, ACS Appl. Mater. Interfaces 7 (2015) 1207-1218.

[17] D. Guo, S. Han, R. Ma, Y. Zhou, Q. Liu, J. Wang, Y. Zhu, In situ formation of iron-cobalt sulfides embedded in N,S-doped mesoporous carbon as efficient electrocatalysts for oxygen reduction reaction, Microporous Mesoporous Mater. 270 (2018) 1-9.

[18] T. Zhou, R. Ma, Y. Zhou, R. Xing, Q. Liu, Y. Zhu, J. Wang, Efficient N-doping of hollow core-mesoporous shelled carbon spheres via hydrothermal treatment in ammonia solution for the electrocatalytic oxygen reduction reaction, Microporous Mesoporous Mater. 261 (2018) 88-97.

[19] T. Zhou, Y. Zhou, R. Ma, Z. Zhou, G. Liu, Q. Liu, Y. Zhu, J. Wang, Nitrogen-doped hollow mesoporous carbon spheres as a highly active and stable metal-free electrocatalyst for oxygen reduction, Carbon 114 (2017) 177-186.

[20] T. Zhou, Y. Zhou, R. Ma, Z. Zhou, G. Liu, Q. Liu, Y. Zhu, J. Wang, In situ formation of nitrogen-doped carbon nanoparticles on hollow carbon spheres as efficient oxygen reduction electrocatalysts, Nanoscale 8 (2016) 18134-18142.

[21] J. Gao, N. Ma, J. Zhai, T. Li, W. Qin, T. Zhang, Z. Yin, Polymerizable Ionic Liquid as

Nitrogen-Doping Precursor for Co–N–C Catalyst with Enhanced Oxygen Reduction Activity, Ind. Eng. Chem. Res. 54 (2015) 7984-7989.

[22] S. Gupta, D. Tryk, I. Bae, W. Aldred, E. Yeager, Heat-treated

polyacrylonitrile-based catalysts for oxygen electroreduction, J. Appl. Electrochem. 19 (1989) 19-27.

[23] V.S. Bagotzky, M.R. Tarasevich, K.A. Radyushkina, O.A. Levina, S.I. Andrusyova, Electrocatalysis of the oxygen reduction process on metal chelates in acid electrolyte, J. Power Sources 2 (1978) 233-240.

[24] H. Jahnke, M. Schönborn, G. Zimmermann, Organic dyestuffs as catalysts for fuel cells, in: F.P. Schäfer, H. Gerischer, F. Willig, H. Meier, H. Jahnke, M. Schönborn, G.

Zimmermann (Eds.) Physical and Chemical Applications of Dyestuffs, Springer Berlin Heidelberg, Berlin, Heidelberg, 1976, pp. 133-181.

[25] D. Singh, J. Tian, K. Mamtani, J. King, J.T. Miller, U.S. Ozkan, A comparison of N-containing carbon nanostructures (CN_x) and N-coordinated iron–carbon catalysts (FeNC) for the oxygen reduction reaction in acidic media, J. Catal. 317 (2014) 30-43.

[26] U. Tylus, Q. Jia, K. Strickland, N. Ramaswamy, A. Serov, P. Atanassov, S. Mukerjee,

Elucidating Oxygen Reduction Active Sites in Pyrolyzed Metal–Nitrogen Coordinated Non-Precious-Metal Electrocatalyst Systems, J. Phys. Chem. C 118 (2014) 8999-9008.

[27] U.I. Kramm, I. Herrmann-Geppert, J. Behrends, K. Lips, S. Fiechter, P. Bogdanoff, On an Easy Way To Prepare Metal–Nitrogen Doped Carbon with Exclusive Presence of MeN_4-type Sites Active for the ORR, J. Am. Chem. Soc. 138 (2016) 635-640.

[28] Y. Hu, O. Jensen Jens, W. Zhang, N. Cleemann Lars, W. Xing, J. Bjerrum Niels, Q. Li,

Hollow Spheres of Iron Carbide Nanoparticles Encased in Graphitic Layers as Oxygen Reduction Catalysts, Angew. Chem. Int. Ed. 53 (2014) 3675-3679.

[29] I.S. Amiinu, X. Liu, Z. Pu, W. Li, Q. Li, J. Zhang, H. Tang, H. Zhang, S. Mu, From 3D ZIF Nanocrystals to Co–N_x/C Nanorod Array Electrocatalysts for ORR, OER, and Zn–Air Batteries, Adv. Funct. Mater. 28 (2017) 1704638.

[30] T. Wang, Z. Kou, S. Mu, J. Liu, D. He, I.S. Amiinu, W. Meng, K. Zhou, Z. Luo, S. Chaemchuen, F. Verpoort, 2D Dual-Metal Zeolitic-Imidazolate-Framework -(ZIF)-Derived Bifunctional Air Electrodes with Ultrahigh Electrochemical Properties for Rechargeable Zinc–Air Batteries, Adv. Funct. Mater. 28 (2017) 1705048.

[31] Y. Chen, S. Jie, C. Yang, Z. Liu, Active and efficient Co-N/C catalysts derived from cobalt porphyrin for selective oxidation of alkylaromatics, Appl. Surf. Sci. 419 (2017) 98-106.

[32] S. Guo, S. Zhang, L. Wu, S. Sun, Co/CoO Nanoparticles Assembled on Graphene for Electrochemical Reduction of Oxygen, Angew. Chem. Int. Ed. 51 (2012) 11770-11773.

[33] Y. Liang, Y. Li, H. Wang, J. Zhou, J. Wang, T. Regier, H. Dai, Co_3O_4 nanocrystals on graphene as a synergistic catalyst for oxygen reduction reaction, Nat. Mater. 10 (2011) 780.

[34] H. Wang, Y. Liang, Y. Li, H. Dai, Co_{-x}S–Graphene ybrid: A igh Performance Metal Chalcogenide Electrocatalyst for Oxygen Reduction, Angew. Chem. Int. Ed. 50 (2011) 10969-10972.

[35] H. Jin, J. Wang, D. Su, Z. Wei, Z. Pang, Y. Wang, In situ Cobalt–Cobalt Oxide/N-Doped Carbon Hybrids As Superior Bifunctional Electrocatalysts for Hydrogen and Oxygen Evolution, J. Am. Chem. Soc. 137 (2015) 2688-2694.

[36] Y. Guo, P. Yuan, J. Zhang, Y. Hu, I.S. Amiinu, X. Wang, J. Zhou, H. Xia, Z. Song, Q. Xu, S. Mu, Carbon Nanosheets Containing Discrete Co-N_x-B_y-C Active Sites for Efficient Oxygen Electrocatalysis and Rechargeable Zn–Air Batteries, ACS Nano 12 (2018) 1894-1901.

[37] G. Wu, N.H. Mack, W. Gao, S. Ma, R. Zhong, J. Han, J.K. Baldwin, P. Zelenay, Nitrogen-Doped Graphene-Rich Catalysts Derived from Heteroatom Polymers for Oxygen Reduction in Nonaqueous Lithium–O2 Battery Cathodes, ACS Nano 6 (2012) 9764-9776.

[38] B.Y. Xia, Y. Yan, N. Li, H.B. Wu, X.W. Lou, X. Wang, A metal–organic framework-derived bifunctional oxygen electrocatalyst, Nat. Energy 1 (2016) 15006.

[39] H. Zhou, D. He, A.I. Saana, J. Yang, Z. Wang, J. Zhang, Q. Liang, S. Yuan, J. Zhu, S. Mu, Mesoporous-silica induced doped carbon nanotube growth from metal–organic frameworks, Nanoscale 10 (2018) 6147-6154.

[40] M. Lefèvre, E. Proietti, F. Jaouen, J.-P. Dodelet, Iron-Based Catalysts with Improved Oxygen Reduction Activity in Polymer Electrolyte Fuel Cells, Science 324 (2009) 71.

[41] F. Xu, Z. Tang, S. Huang, L. Chen, Y. Liang, W. Mai, H. Zhong, R. Fu, D. Wu, Facile synthesis of ultrahigh-surface-area hollow carbon nanospheres for enhanced adsorption and energy storage, Nat. Commun.6 (2015) 7221.

[42] Y. Qian, Z. Liu, H. Zhang, P. Wu, C. Cai, Active Site Structures in Nitrogen-Doped

Carbon-Supported Cobalt Catalysts for the Oxygen Reduction Reaction, ACS Appl. Mater. Interfaces 8 (2016) 32875-32886.

[43] W. He, C. Jiang, J. Wang, L. Lu, High-Rate Oxygen Electroreduction over Graphitic-N Species Exposed on 3D Hierarchically Porous Nitrogen-Doped Carbons, Angew. Chem. Int. Ed. 53 (2014) 9503-9507.

[44] J.-S. Li, S.-L. Li, Y.-J. Tang, M. Han, Z.-H. Dai, J.-C. Bao, Y.-Q. Lan, Nitrogen-doped Fe/Fe_3C@graphitic layer/carbon nanotube hybrids derived from MOFs: efficient bifunctional electrocatalysts for ORR and OER, Chem. Commun. 51 (2015) 2710-2713.

[45] L. Lai, J.R. Potts, D. Zhan, L. Wang, C.K. Poh, C. Tang, H. Gong, Z. Shen, J. Lin, R.S. Ruoff, Exploration of the active center structure of nitrogen-doped graphene-based catalysts for oxygen reduction reaction, Energy Environ. Sci. 5 (2012) 7936-7942.

[46] J.M. Ziegelbauer, T.S. Olson, S. Pylypenko, F. Alamgir, C. Jaye, P. Atanassov, S. Mukerjee, Direct Spectroscopic Observation of the Structural Origin of Peroxide Generation from Co-Based Pyrolyzed Porphyrins for ORR Applications, J. Phys. Chem. C 112 (2008) 8839-8849.

[47] X. Zhong, L. Liu, Y. Jiang, X. Wang, L. Wang, G. Zhuang, X. Li, D. Mei, J.g. Wang, S. Su Dang, Synergistic Effect of Nitrogen in Cobalt Nitride and Nitrogen oped ollow Carbon Spheres for the Oxygen Reduction Reaction, Chem. Cat. Chem. 7 (2015) 1826-1832.

[48] . u, . Yang, C. Wang, Y. Zhang, . Lu, Q. Wang, Co N oped Mesoporous Carbon Hollow Spheres as Highly Efficient Electrocatalysts for Oxygen Reduction Reaction, Small 13 (2016) 1602507.

[49] Y. Zheng, Y. Jiao, J. Chen, J. Liu, J. Liang, A. Du, W. Zhang, Z. Zhu, S.C. Smith, M. Jaroniec, G.Q. Lu, S.Z. Qiao, Nanoporous Graphitic-C_3N_4@Carbon Metal-Free Electrocatalysts for Highly Efficient Oxygen Reduction, J. Am. Chem. Soc. 133 (2011) 20116-20119.